Structures, Structural Dynamics, and Materials and Co-located Conferences
April 8-11, 2013, Boston, Massachusetts
54th AIAA/ASME/ASCE/AHS/ASC Structures, Structural Dynamics, and Materials Conference

10.2514/6.2013-1672

Deployment Modeling and Experimental Testing of a Bi-stable Composite Boom for Small Satellites

Pau Mallol* and Gunnar Tibert†
Royal Institute of Technology (KTH), SE-100 44 Stockholm, Sweden

The rapidly growing use of nano- and pico-satellites for space missions requires deployable systems to be highly storable yet large and with adequate mechanical properties when deployed. This paper focuses on the modeling and simulation of a meter-class passively deployable boom – based on the SIMPLE boom by Thomas W. Murphey – exploiting the bi-stable nature of composite shells. Experimental tests were also carried on a boom prototype suspended in a gravity off-loading system. The strain energy level, deployment time and spacecraft displacements of the models agree well with analytical analyses, confirming the theoretical accuracy of the finite element model. However, the simulations show that the boom deploys six times faster than the real prototype. The quick deployment and violent end-of-deployment shock provokes the boom deployment dynamics to be unrealistic but still shows a reasonable behavior given the nature of the deployment. Future improvements in the material and friction models will, most likely, provide us with a more realistic finite element model.

Nomenclature

ACS	= Attitude Control System
SIMPLE	= Self-contained linear meter-class deployable boom
GFRP	= Glass Fibre Reinforced Polymer
CFRP	= Carbon Fibre Reinforced Polymer
GOLS	= Gravity Off-Loading System
MoI	= Moment of Inertia
FEA	= Finite Element Analysis
DOF	= Degree of Freedom

I. Introduction

A. CubeSat history

THE CubeSat form-factor was created in 2000 by CalPoly and Stanford University. The aim was to give universities the capacity of developing small satellites at a reasonable cost and to provide to the scientific community a new alternative for their missions. The basic CubeSat configuration is named 1U, which has a standard size of 100 × 100 × 100 mm^3 and an approximate mass of 1 kg, although larger configurations are today available: 1.5U (100 × 100 × 150 mm^3), 2U (100 × 100 × 200 mm^3), 3U (100 × 100 × 300 mm^3), 4U (100 × 100 × 400 mm^3), 5U (100 × 100 × 500 mm^3), and 6U (100 × 200 × 300 mm^3):

> An 8 kg 6U CubeSat can be designed to perform some of the Earth observation missions of 100 kg micro-satellites. A 6U CubeSat…has 4 times the payload capacity of a 3U CubeSat…which uses two thirds of its volume for system components. [1]

In the last decade well over 50 CubeSat missions have been launched and more than 20 are planned to take off in the next few years. [2] Although the current success rate of the CubeSat missions lies around 50 % including launcher failures, like the DNEPR where 14 CubeSats were destroyed at once in July 2006, CubeSat missions are already an extremely valuable platform for universities and the scientific community.

A 1U CubeSat usually weighs up to approximately 1 kg (pico-satellite class) and the larger configurations fall into the nano-satellite class (1–10 kg). In this paper we will use the terms pico-satellite, nano-satellite, and CubeSat indifferently since our work is relevant for any small satellite.

* PhD student, Dept. of Mechanics, Osquars backe 18, AIAA Student Member.
† Associate Professor, Dept. of Mechanics, Osquars backe 18, AIAA Senior Member.

B. CubeSat motivation

The CubeSat missions are excellent platforms for educational organizations to involve students in a real and complete space mission. It provides an enormous flexibility to perfectly suit almost any program syllabus (electronics, mechanics, computer science, etc.) especially because off-the-shelf components are readily available permitting the students to focus on developing the systems that match their program. Furthermore, CubeSat projects have a very short development time, usually less than three years, allowing the students to be involved in the project from the very beginning until the launch.

Another important benefit is that CubeSats also drastically lowers the launching costs thanks to the standardized P-POD (Poly Pico-satellite Orbital Deployer) module. It also usually allows a better filling of the fairing of the launcher with useful payloads (thus optimizing the launcher's use). From the mission type point of view, such small spacecraft makes real-time multipoint measurements affordable, which is a very interesting and useful measurement method for many scientific disciplines. A relevant example is the QB50 mission, an international network of about 50 CubeSats for multi-point, in-situ measurements in the lower thermosphere (90–320 km altitude) and re-entry research.

C. Deployable systems for small satellites

Small satellites with less than 10 kg mass already are attractive for many research areas:

> A considerable number of CubeSats have been launched, the majority of them being demonstration or educational missions…The market for nano-satellites and activity in this field are growing rapidly. Driving the development in the high-end of the market will allow the SMEs' [Small and Medium Enterprises] consortium to offer the scientific agencies a low cost alternative (compared to traditional satellites) to a range of scientific missions. This will contribute to creating a vital and sustainable market for nano-satellites beyond educational missions. [3]

The electronic systems miniaturization and integration density combined with the decrease of spacecraft's volume indicates that the current bottlenecks are the stowed volume and mass of deployable structures. It is a great challenge to decrease the actual packaging volume of such systems but it is necessary to fully exploit all the potential of low cost small satellites. In the deployable structures area, large efforts are being made to develop highly storable, yet large, deployable structures like solar sails, trusses or booms. [4,5] Some notable examples of deployable booms for small satellites are STEM (Storable Tubular Extendible Member by Astro Aerospace), TRAC (Triangular Retractable and Collapsible boom by AFRL, Air Force Research Laboratory, [6,7]), CTM (Collapsible Tubular Mast by DLR [8]), STACER (Spiral Tube and Actuator for Controlled Extension and Retraction by Surrey Satellite Technology Ltd. [9]), and SIMPLE (Self-contained Linear Meter-class deployable by AFRL). [10]

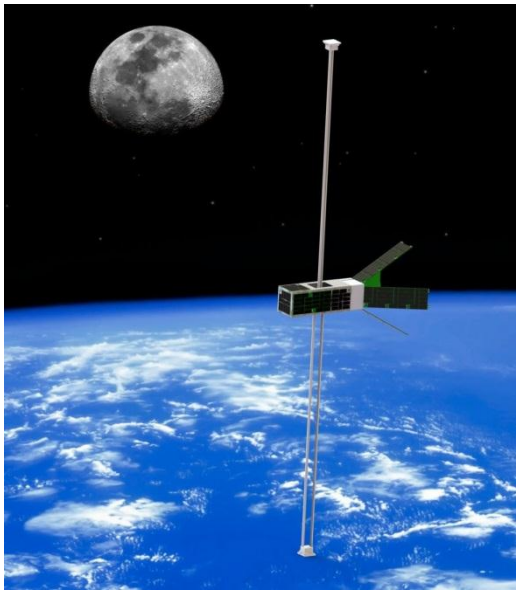

Figure 1. SEAM (Small Explorer for Advanced Missions) artistic view. *A 3U CubeSat with a pair of one meter deployable SIMPLE booms.* [3]

Besides power, data processing hardware, communication systems, etc. a common mission scenario is the requirement that scientific equipment is placed away from the main satellite (e.g. magnetometers, which would get affected by the inherent electromagnetic effects of the satellite electronic hardware). In these cases a deployable system is necessary, Fig. 1. This requirement creates new constraints on the satellite development. The most important are:

1) **Volume**: difficulty to compactly stow relatively large, compared with the main satellite size, deployable structures. This limitation is emphasized if the stowed structure possesses a large level of strain energy stored as risk of accidental deployment needs to be mitigated with robust stowing containers, usually meaning extra volume and mass.
2) **Power**: limited power available for deployment control. If a passive deployment scheme is used, modeling, simulation, and testing phases become, in many cases, greater challenges than for active deployable systems, i.e. due to the need of a good understanding and prediction of such systems.
3) **Attitude**: due to the attitude control limitations of CubeSats, the end-of-deployment shock and posterior boom dynamics can represent attitude challenges if they exceed the control capacity of the attitude control system, especially with passive ACS schemes.

4) **Stiffness and relative position**: bi-stable booms are usually made of thin composite materials which can be easily bent. In cases where sensors, e.g. magnetometers, are placed in the tip of the boom, the deployed boom stiffness and relative orientation of the tip needs to be carefully analyzed and predicted. The main natural frequencies of the boom need also to be analyzed and ensure that they are not close to spacecraft on-orbit disturbances.

The SIMPLE boom by Thomas W. Murphey (US Patent Pending, Application #12957495), inspired KTH's boom design and the work presented here. It is a meter-class boom that exploits the bi-stable nature of GFRP (Murphey's design) or CFRP (KTH's design) ultrathin composite shells, which gives a stable configuration in both the stowed and deployed configurations. The strain energy levels at the stowed configuration are relatively low but enough to drive a complete deployment. This type of boom requires little containing hardware and little or no deployment control.

II. Background

D. The CubeSat mission

The SWIM (Space Weather using Ion spectrometers and Magnetometers) mission is a collaboration project between IAUPR (Inter American University of Puerto Rico), UF (University of Florida), AFRL, and KTH to develop a 3U CubeSat mainly for studying the space weather at low Earth orbits, between 500 and 600 km altitude. Among other hardware there is SMILE (Small Magnetometer In Low mass Experiment), a magnetometer monitoring the magnetic field on the vicinity of the SWIM CubeSat for studying auroral regions and also as part of the attitude control system. [11] SMILE needs to be placed at one meter, or further, from the CubeSat to avoid electromagnetic interferences thus a deployable boom is used. The magnetic field data from SMILE are also used for spacecraft's attitude determination and it is crucial that the boom that has appropriate structural properties when deployed to keep SMILE within the required orientation margins.

E. Bi-stable tape springs

The term bi-stability refers to a structure that shows two well-defined stable equilibrium configurations. In our case those configurations are the coiled (stowed) and straight (deployed) ones. From the mechanics point of view these two configurations must be the two states with the lowest strain energy (two local minima or energy wells). To transit between both states, activation energy is necessary, e.g. bending moments M in Fig. 2. Extensive work has been done by Pellegrino and Iqbal [12] among other researchers and our analyses are based on their research.

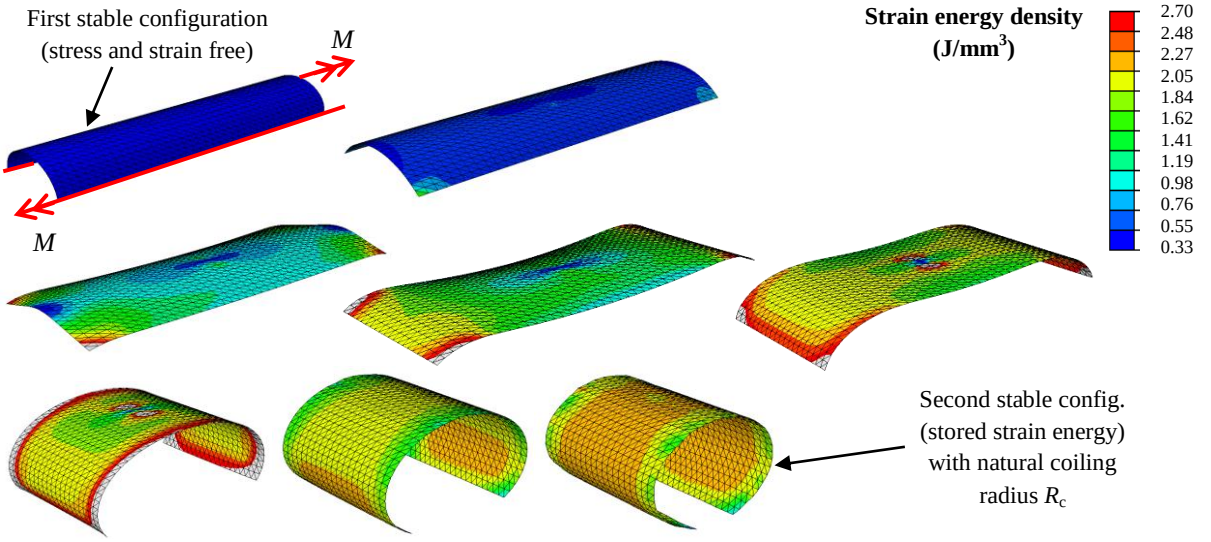

Figure 2. Transition of a bi-stable tape spring between the first stable configuration (straight) and the second one (coiled).

Figure 3 shows the classical strain energy curves for a bi-stable and non-bi-stable tape spring: once a certain applied moment is reached (both points A), the tape spring flattens and then starts coiling on a virtual cylinder that has its axis perpendicular to the straight configuration longitudinal axis, as in Fig. 2. If the applied moment is removed, we might see two effects: in a non-bistable shell it springs back to its initial straight configuration,

point B in Fig. 3, or in the bi-stable tape spring case, it remains coiled storing a certain amount of strain energy. It is the latter case that we exploit, using the stored strain energy for deploying a bi-stable composite boom.

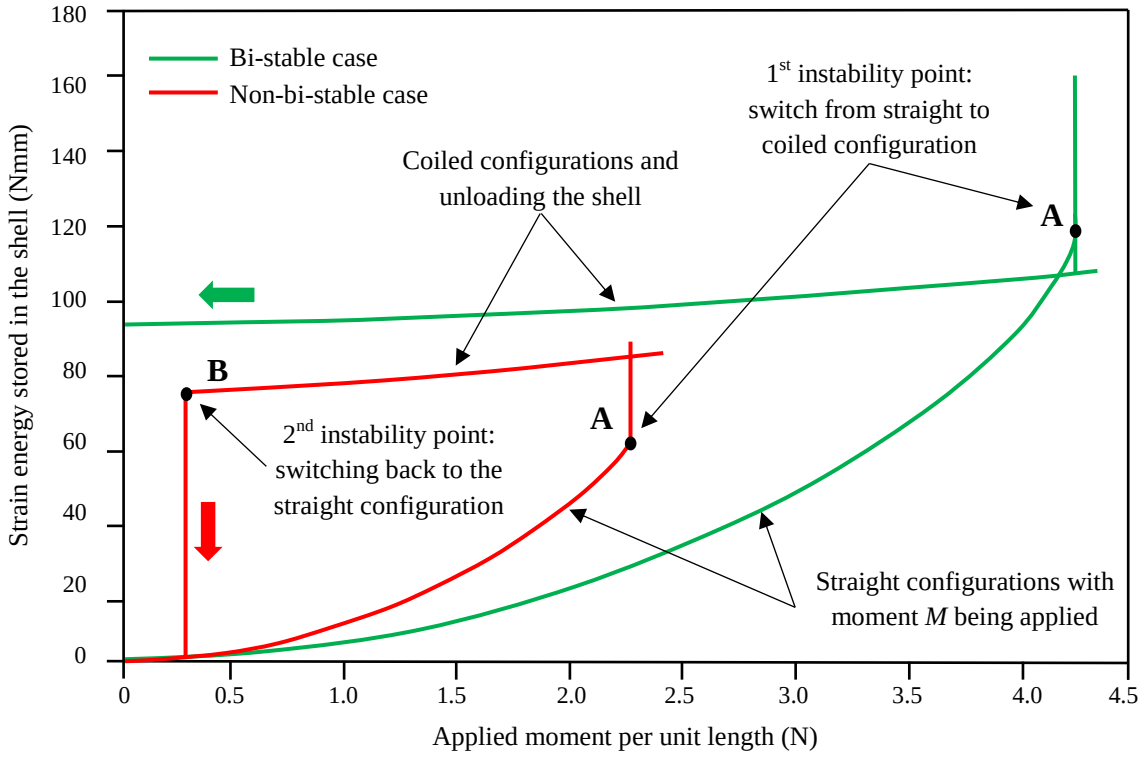

Figure 3. Typical strain energy curves for non-bi-stable and bi-stable tape springs (edited plots from [13]).

F. Boom prototype and SWIM dummy

KTH has built a prototype (Fig. 4) based on the SIMPLE boom. The main objectives were to characterize the boom eigen-frequencies, eigen-modes, and to investigate the deployment dynamics of bi-stable composite booms. Eigen-frequency analyses and experimental vibration tests were performed, [14] but the results are not presented in this paper to focus on the deployment dynamics.

From basic parameters from the SIMPLE boom, [10,15] a suitable CFRP prepreg, i.e. a CFRP ply pre-impregnated with a polymer matrix, was selected and several tape springs manufactured on KTH's premises. The rest of mechanical components like the container, spools, SMILE sensor case and the release mechanism were fabricated using SLS (Selective Laser Sintering) and SLA (Stereolithography Apparatus) additive manufacturing methods directly from CAD models, providing extremely fast yet accurate parts and a quick design iteration process. From available data of the SWIM CubeSat, i.e. total mass, mass distribution, center of gravity, and moments of inertia, a dummy of the spacecraft was also manufactured for preliminary simulated zero-gravity deployment tests.

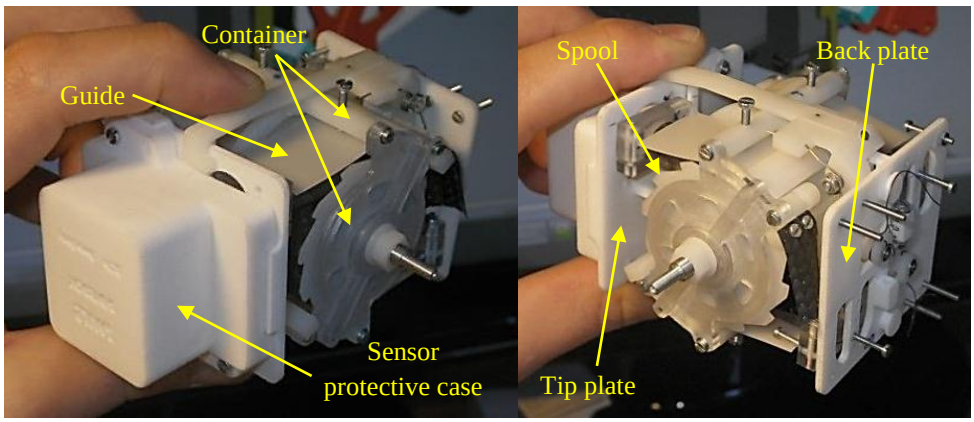

Figure 4. Stowed KTH's boom prototype. *The overall prototype volume is 85 × 60 × 55 mm^3.*

G. Gravity Off-Loading System (GOLS)

The basic requirements for relevant deployment tests are: [16]

1) The dummy satellite, central boom spools, and boom tip mass shall be gravity off-loaded.
2) The boom shall be deployed with minimal resistance from the GOLS.
3) The boom shall be able to vibrate relative to the satellite dummy.

Using a GOLS and 10 m long fishing lines to hold the boom and satellite dummy, Fig. 5, fulfills requirements 1 and 2: the work done by the horizontal components of the forces in the fishing lines of the GOLS during deployment is minimized for d = 0.37 m. With the current GOLS set-up requirement 3 is partially fulfilled. The main source of the current limitations is the coupling between the very soft springs that hold the boom and the spring for the dummy satellite. Relevant limitations in the GOLS due to activation of springs are:

1) Limited rotation in the vertical longitudinal plane.
2) Limited rotation in the horizontal plane.

III. Experiments

H. Deployment tests set-up

With the boom prototype, satellite dummy, and the GOLS, preliminary deployment tests were set up, Fig. 6. The main objectives of the deployment tests were:

1) Observe the fundamental vibration mode of the boom.
2) Compare, qualitatively, the finite element simulations with the experiments in terms of deployment time and boom deployment dynamics.

Preliminary results based on films are shown in Figs. 7 and 8. The deployment took 1.03 s and the first eigen-mode is dominated by combined bending although some torsion is also present.

In Fig. 7 it is shown that with the actual GOLS the CubeSat dummy can rotate in the horizontal plane but all the springs of the GOLS are activated thus absorbing energy from the system. The rotation in the horizontal plane as seen in Fig. 7 is caused by the fact that all the masses need to be suspended, this means each attachment point between the boom or CubeSat dummy and the GOLS generates reaction moments. These reactions moments will be minimized in a future GOLS version. Note that due to the principle of conservation of angular momentum, this rotation is not seen in the Abaqus simulations or in an on-orbit deployment.

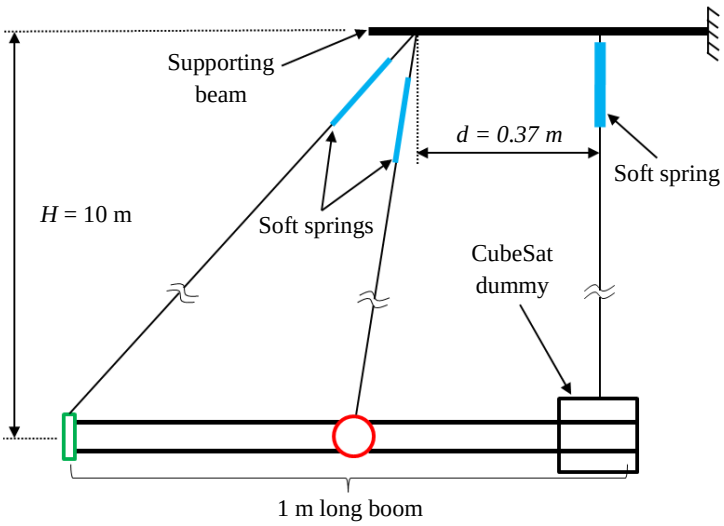

Figure 5. Gravity Off-Loading System. *Scheme not to scale*. [16]

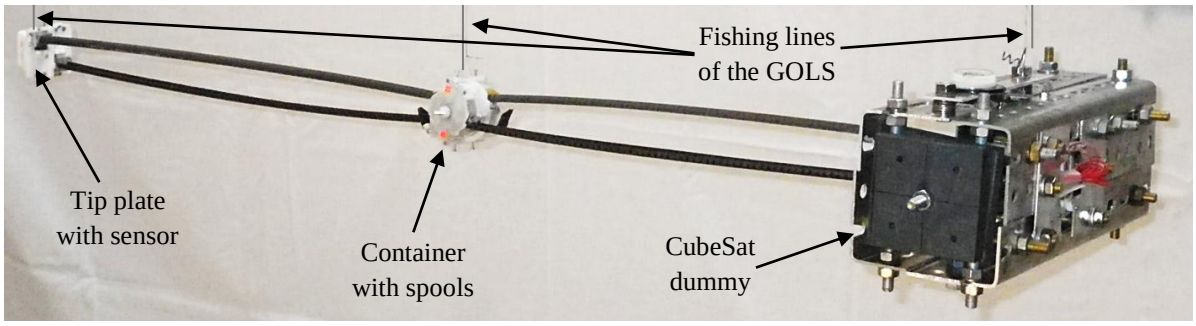

Figure 6. Deployed boom and CubeSat dummy suspended from the GOLS.

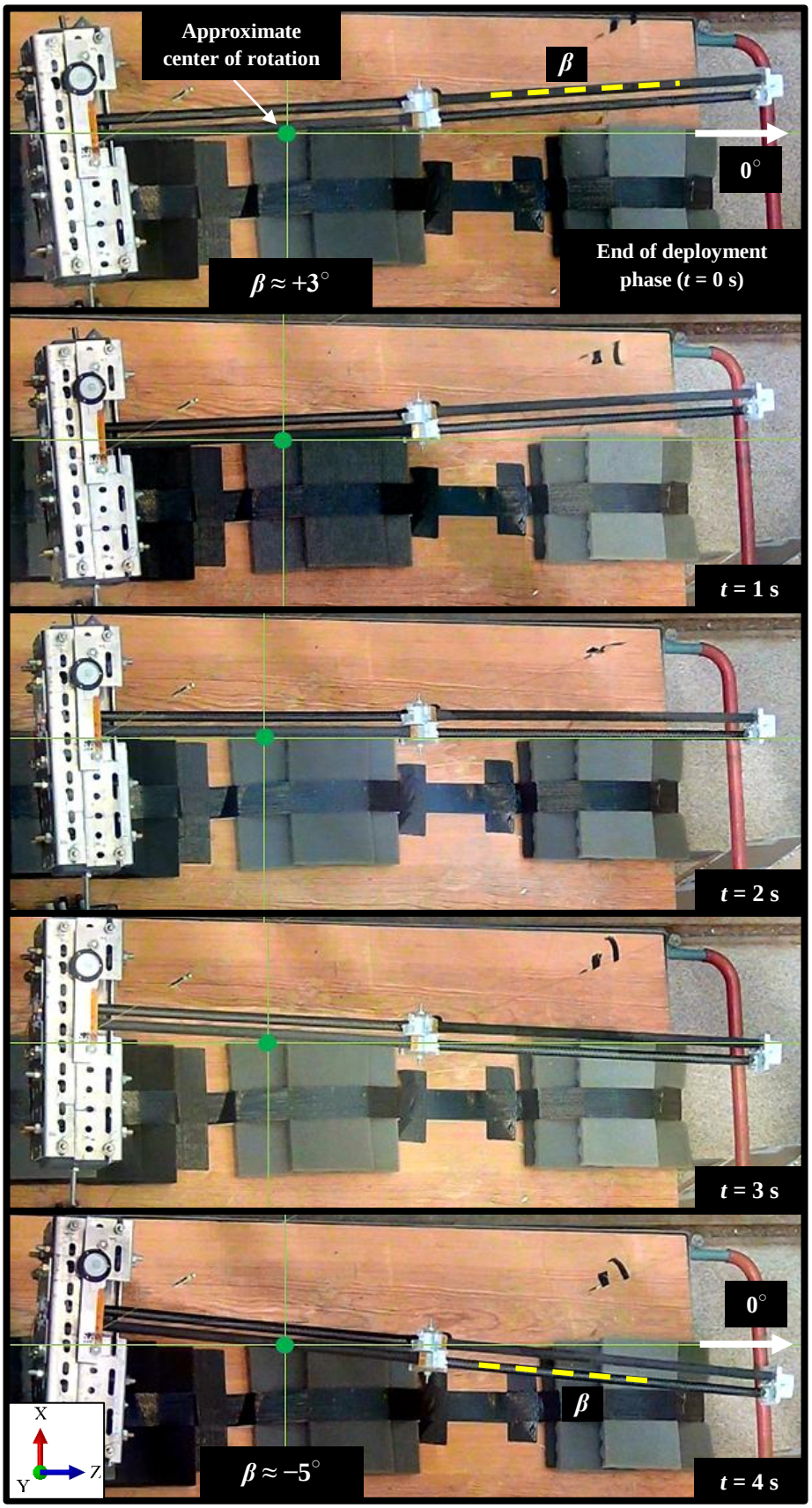

Figure 7. Horizontal boom rotation after the end-of-deployment shock (upper view).

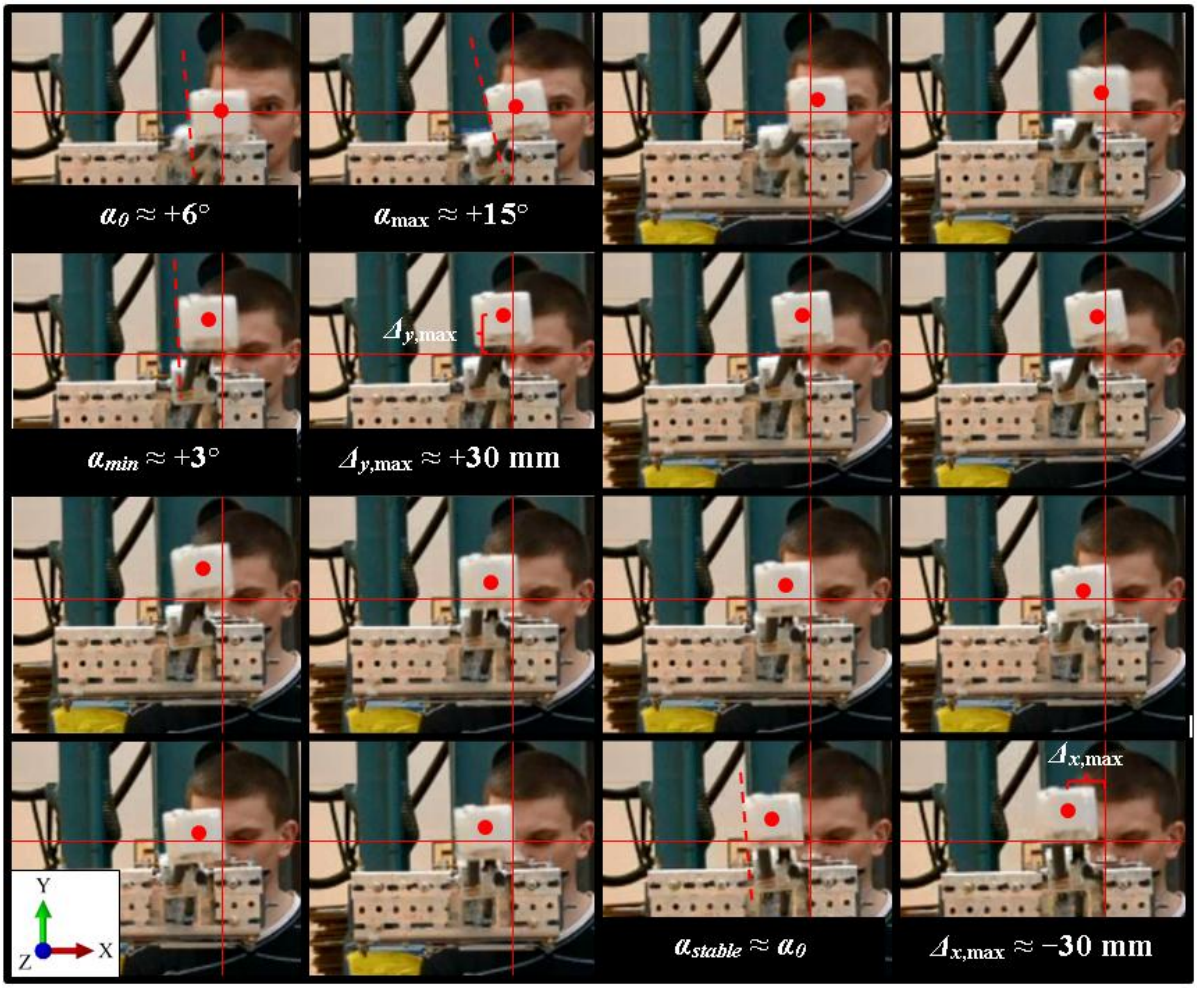

Figure 8. Shock and post-deployment dynamics of the boom (front view). *Each snapshot has a time difference of 0.1 s and the total time span in this sequence is 1.5 s.*

IV. Abaqus simulations

I. Boom modeling and deployment simulations

Our boom laminate consisted of a single woven ply of CFRP, a Twill 2×2 prepreg of high strength T300 carbon fibers in a 120 °C toughened epoxy matrix. From the material point of view, the main modeling difficulties come from the orthotropic nature of this material and the woven structure embedded in the epoxy matrix. The main properties of the Twill 2×2 used were (nominal values from the manufacturer's datasheet unless otherwise stated):

- Manufacturer's product name: *HexPly® M49/42%/200T2X2/CHS-3K*
- Fiber areal mass: 0.200 kg/m^2
- Fiber density: 1780 kg/m^3
- Resin density: 1180 kg/m^3
- Cured thickness (measured and averaged): 0.24 mm
- Young modulus: 63 GPa (this value corresponds to a multi-layer laminate, standard test EN 2561 B).
- Flexural modulus: 56 GPa (this value corresponds to a multi-layer laminate, standard test EN 2562)

MATERIAL MODELING

Modeling the internal structure of woven composites is complex and computationally expensive. Another added complication when modeling thin FRP (Fiber Reinforced Polymer) is the difficulty to get thin composite in- and out-of-plane mechanical properties. The standards commonly used for creating the FRP datasheets are designed to be used in multi-ply laminates and it is not usually possible to extract accurate single ply properties

from them. There are several possibilities to solve or mitigate the mentioned problems, the main ones considered were:

1) Model a representative volume element (RVE) of the woven composite (e.g. using TexGen [17] and Abaqus), derive the homogenized elastic mechanical properties and plug them in an Abaqus material model. [18]
2) Use the homogenization technique [19] in a composite unit cell approximating the internal structure with beam elements and multipoint constraints, extract the ABD matrix coefficients of the composite and assign the elastic properties in material model in Abaqus.
3) To model the woven structure as a series of unidirectional FRP plies and isotropic layers and tune ply thicknesses and positions across the laminate thickness to match the real available material properties. [20]

The current material model is based on case 3. We defined two ply materials, an isotropic epoxy and a unidirectional CFRP ply. The isotropic epoxy material has the following properties: density ρ = 1180 kg/m^3, Poisson's ratio v = 0.3, and Young's modulus E = 10.04 GPa

To define the unidirectional CFRP material we used an orthotropic model, which uses the principal directions 1, 2, and 3 to define its mechanical properties: direction 1 corresponds to the fibers direction, 2 is the direction perpendicular to the fibers (in-plane), and 3 is the thickness direction. The unidirectional (UD) ply in our models have an overall material density ρ = 1780 kg/m^3, Poisson's ratio v_{12} = 0.15, Young's moduli E_1 = 164.01 GPa, E_2 = 10.04 GPa, and the three shear moduli $G_{12} = G_{13} = G_{23}$ = 3.86 GPa.

With the two materials defined we created a bi-stable antisymmetric laminate as in Table 1 and a series of simulations were run to tune the layup thicknesses until obtaining:

1) A laminate that shows bi-stability.
2) Bending modulus as close as possible to the real woven CFRP ply used.
3) A natural coiling radius, Fig. 2, as close to 10 mm as possible (boom geometric requirement).
4) A bi-stable laminate that does not uncoil when it is coiled on a cylinder of 15 mm radius (boom geometric requirement).

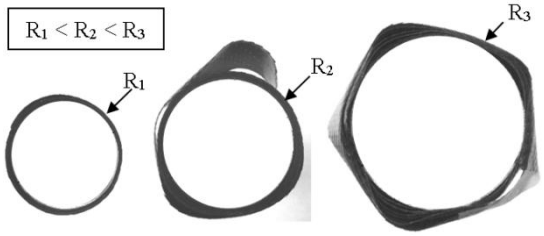

Figure 9. Instability as the coiling radius increases. *Modified figure from Ref. 10.*

As mentioned above, the common standard tests used to find the tensile and flexural strengths as well as moduli of composites are designed for thick laminates, for instance 2±0.2 mm for EN ISO 14125, meaning 6 or 7 layers with the composite material we use.

Bi-stability highly depends on the material bending properties thus we performed a series of basic three-point bending tests to approximate our material model to the Twill 2×2 of the boom (condition 2). The single-ply coupons of interest here, had the fiber bundles oriented at 45° and we found that our material had a bending modulus of about 5.5 GPa. Tensile tests were also performed to find the tensile modulus of 9.9 GPa. With this data we tuned the Abaqus laminate to the real material.

Since the boom spools where the tape springs are coiled have a radius of 10 mm, it is important to match as good as possible condition 3. If the natural coiling radius of the tape spring is too large the tape springs will not embrace the spools properly; if the tape spring model uncoils below the 15 mm radius in the complete boom model the outer layers of the coiled tape springs will start blooming inside the container (unstable coiling, Fig. 9). From the geometric dimensions of our boom, the final radius of the coiled tape springs becomes 14.1 mm and it is stable. Having a laminate that does not spontaneously uncoil on a 15 mm radius cylinder (condition 4) avoids simulation problems and an unrealistic model. The laminate in Table 1 showed to have a natural coiling radius of 8.9 mm and stability on a 15 mm radius cylinder.

Table 1. Laminate parameters used to approximate the boom material.

Layer number	Material	Layer thickness (mm)	Rotation angle (°)
1	Epoxy	0.0145	0
2	UD ply	0.0512	+45
3	UD ply	0.0512	−45
4	Epoxy	0.0062	0
5	UD ply	0.0512	+45
6	UD ply	0.0512	−45
7	Epoxy	0.0145	0

BOOM PHYSICAL PARAMETERS

We have mainly investigated two models (Fig. 10):

Case 1: boom with no spacecraft and one tip fixed, i.e. the standalone boom.

Case 2: boom attached to a CubeSat model and free-free deployment.

The boom assembly consists of two spools within the container part, Figs. 4 and 11, two pairs of 500 mm long tape springs each attached to the spools (one spool for each pair), a tip plate with a sensor (the latter it was not modeled but its mass and MoI included in the tip plate), and fixed plate for the standalone boom model and substituted by a Cubesat model in the free-free simulations. The masses and MoI that need to be manually set are listed in Table 2. The tape springs mass (0.006 kg/m) and MoI are calculated internally in Abaqus from the part material and section properties. The main geometric properties of each part are:

1) Tape spring: 500 mm long semi-cylindrical shell with internal radius R_{tape} = 6.35 mm and subtended angle β = 180º. Note that in the assembly there is a 2.5 mm overlap in the spools attachment that gives a total deployed boom length, from tip plate to tip plate, of 995 mm.
2) Spool: 10 mm radius and 22 mm wide cylinder with 15.7 mm radius lateral discs.
3) Container with guides: 16 mm radius and 44 mm wide cylinder with guides.
4) Tip plates: 50 × 50 mm^2 square planar shell.

Table 2. Masses and moments of inertia of each part with respect to its center of mass.

Part	Mass ($\cdot 10^{-3}$ kg)	I_{xx} (kgm^2)	I_{yy} (kgm^2)	I_{zz} (kgm^2)
Spool	8	$0.86 \cdot 10^{-6}$	$1.88 \cdot 10^{-6}$	$1.88 \cdot 10^{-6}$
Container	18	$9.2 \cdot 10^{-6}$	$8.6 \cdot 10^{-6}$	$11.7 \cdot 10^{-6}$
Tip plate with SMILE sensor	48	$11.4 \cdot 10^{-3}$	$11.4 \cdot 10^{-3}$	$12.8 \cdot 10^{-6}$
Fixed tip	16	$4.9 \cdot 10^{-3}$	$4.9 \cdot 10^{-3}$	$7.6 \cdot 10^{-6}$
CubeSat	2700	0.04	0.77	0.74

COILING PHASE

Once a suitable material model is found it can be plugged into a boom model to simulate the coiling procedure and the posterior boom deployment. The simulation of a complete coiling is important to store a realistic value for the strain energy in the tape springs which strongly affect the deployment speed and posterior dynamics. That is due to the fact that the greater stored strain energy in the coiled part of the boom, the greater strain energy gradient in each transition zone is, which provides the deployment force. The transition zone, Fig. 11, is usually defined as the tape spring length between the two sections of the boom with zero Gaussian curvatures, i.e. a cylindrical shape, which are the completely deployed and coiled states. The coiling phase sequence is also shown in Fig. 12, phase that is the same in both cases 1 and 2.

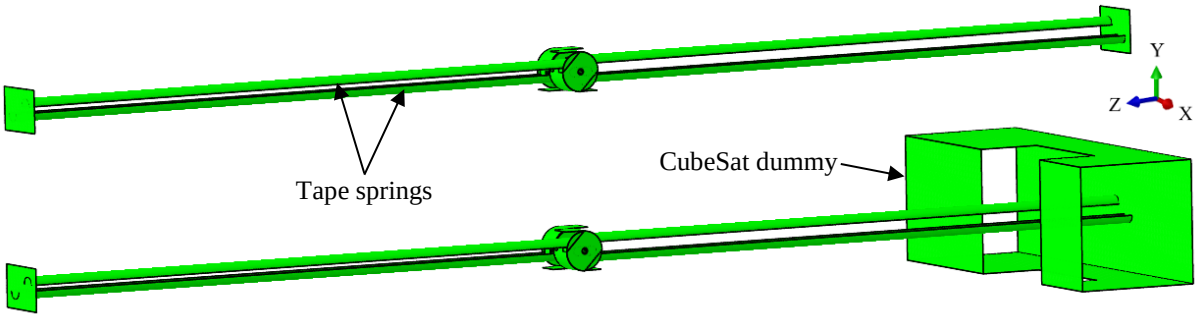

Figure 10. Simulated models. *Standalone boom with one tip plate fixed (case 1, upper model) and boom on a CubeSat model for free-free simulations (case 2, lower model).*

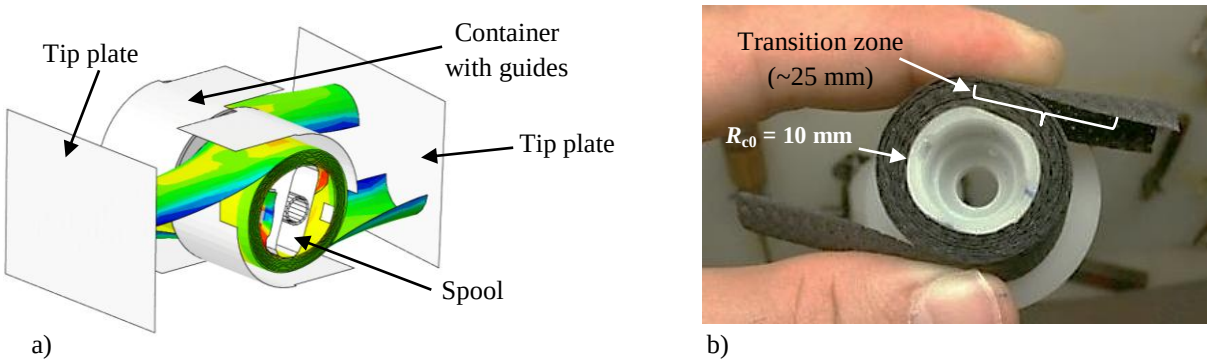

Figure 11. Section cut of the coiled tape springs in Abaqus, a), and two CFRP tape springs coiled on the spool of the boom prototype, b).

It is important to note that between the end of the coiling phase and deployment there is a phase we call "relaxation" that, constraining both boom tips and the container (the spools are free to rotate) aims at "relaxing" the coiled tape springs to their natural shape within the container part. After this relaxation phase, all the constraints are released to simulate a free-free deployment (case 2) or one tip plate is kept fixed (case 1).

DEPLOYMENT PHASE

After the coiling and relaxation phases are completed, a deployment can be simulated releasing all constraints but the ones needed for each studied case. In both cases, different friction values, contacts, and boundary conditions combinations have been studied but for space limitation we will only present four of them in this paper:

Case 1a. Standalone boom with one tip plate fixed and no friction.

Case 1b. Standalone boom with one tip plate fixed and a friction coefficient of 0.2 between tape springs and container.

Case 2a. Boom in a CubeSat dummy model with no friction and free-free deployment.

Case 2b. Boom in a CubeSat dummy model with a friction coefficient of 0.2 between tape springs and container and free-free deployment.

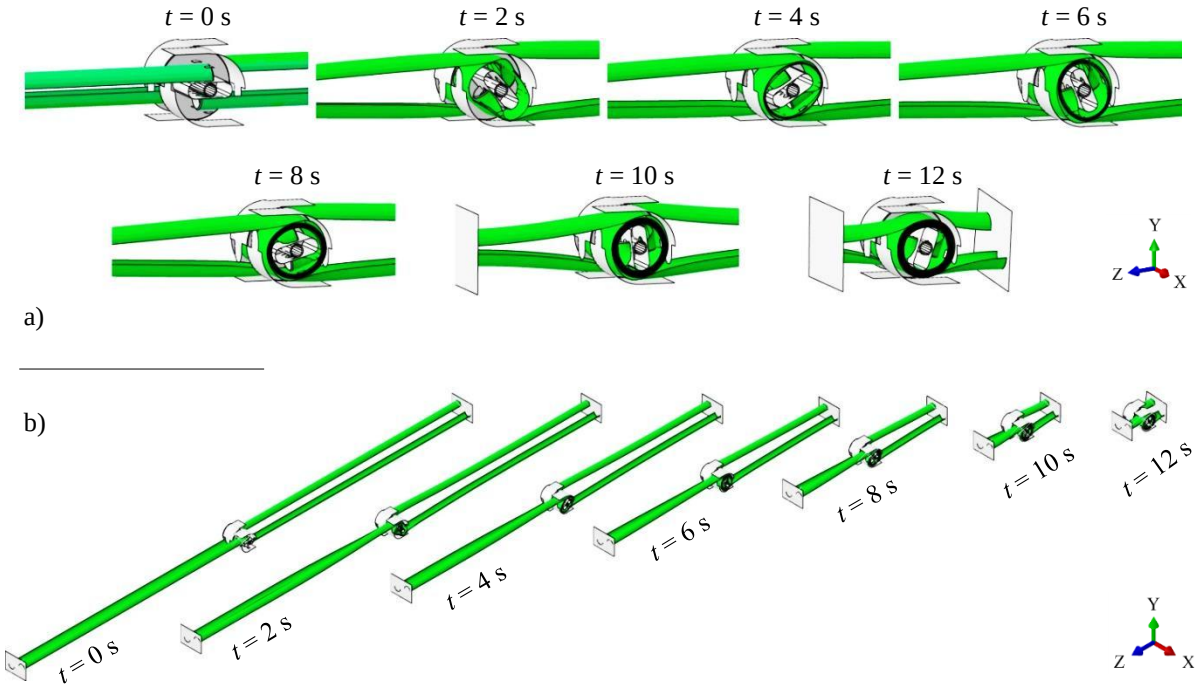

Figure 12. Coiling sequence of the boom without CubeSat. *The coiling sequence is essentially the same for all four cases presented in this paper.*

V. Results

This section presents a selection of analyses and results from the four Abaqus cases as well as experimental tests. Analytical models to estimate the total strain energy stored after coiling, deployment time and CubeSat longitudinal displacement during deployment are presented and compared with the Abaqus results (Table 3). Free tip displacements during deployment and overall kinetic energy profiles are plotted and compared between simulated cases. Finally, deployment and post-deployment sequences of all four cases until the models reached a final deployed state are depicted. In Fig. 13 we depict the legend of symbols used in the figures.

Table 3. Relevant simulation results to compare with the analytical models.

Parameter	Case 1a	Case 2a	Case 1b	Case 2b
Stowed boom longitudinal length (mm)	94	88	95	86
Stored strain energy (J)	8.3	8.9	8.2	9.1
CubeSat longitudinal displacement during deployment (mm)	N/A	31	N/A	23
Deployment time (s)	0.11	0.12	0.13	0.15

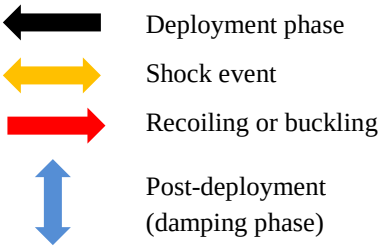

Figure 13. Legend used in subsequent plots.

J. Stored strain energy

Pellegrino and Iqbal [12] developed an analytical model to characterize bi-stable laminates. This model has been used to calculate an estimator of the total stored strain energy in our finite element boom model. Since the strains due to stretching are much smaller than the bending strains, only the latter has been included in our analysis. The input parameters used are:

1) Tape springs: internal radius R_{tape} = 6.35 mm, subtended angle β = 180º, laminate thickness h_{tape} = 0.24 mm, and effective coiled length L_{tape} = 450 mm.
2) Spool: 10 mm radius (= R_{c0} for the first coiled section).
3) Material properties: $D_{11} = D_{22} = 2.8 \cdot 10^{-2}$ Nm, $D_{12} = 0.8 \cdot 10^{-2}$ Nm, which are the required ABD matrix coefficients for the analytical model used in this section.

During the coiling phase the effective coiling radius (R_c) varies since the tape springs coil on each other. To account for that aspect R_c has been substituted for a function $R_c = f(\phi)$, where ϕ is the angle that the spool has already turned during coiling. The final angular rotation when the boom is totally stowed is ϕ_{cf} =38.7 rad. This value agrees well with the Abaqus coiling angle of 37.6 rad, the differences likely come from the fact that in the Abaqus model the tapes coils are not always in contact, building up some extra radius in every new coil, which also happens in the real boom.

Given the initial conditions that in the straight (deployed) and coiled configurations the bending strain energy to pass from the straight configuration to the coiled one is [12]

$$\frac{\mathrm{d}U}{\mathrm{d}\phi} = \frac{\pi}{2} R_{\text{tape}} R_c \left[\frac{D_{11}}{R_c^2} - \frac{2D_{12}}{R_{\text{tape}} R_c} + \frac{D_{22}}{R_{\text{tape}}^2} \right] = Q(\phi) \tag{1}$$

where ϕ is the coiling angle. Equation (1) can now be integrated between ϕ = 0 and ϕ_{cf} = 37.6 rad (Abaqus value). The result of this calculation for one single tape spring, from which 450 mm of its total length is coiled, gives a total strain energy stored of $U_{bend,1tape}$ = 2.9 J thus 11.6 J for four tape springs. The total strain energy prior deployment is in the neighborhood of the strain energy values found in Abaqus for the present cases (Table 3).

In Figs. 14–16 the strain energy plots during each simulated case shows that cases 1a and 2b release almost all the strain energy during deployment but not completely, conserving 0.07 J and 0.17 J respectively in the tape springs. Case 1b conserves 1.38 J and 2a 0.75 J due to the highly bent final deployed shape as seen in posterior sections. The same plots show how in the models with the boom fixed in one end, i.e. 1a and 1b, the shock at the end of deployment is more violent, even with less train energy stored than in the equivalent models with CubeSat: 7 % less in the frictionless case and 10 % less in the case with friction. That is caused by the boundary conditions at the fixed plate, aspect that will be commented in section VI. Note that no severe buckling occurred in case 1a but recoiling and a second deployment.

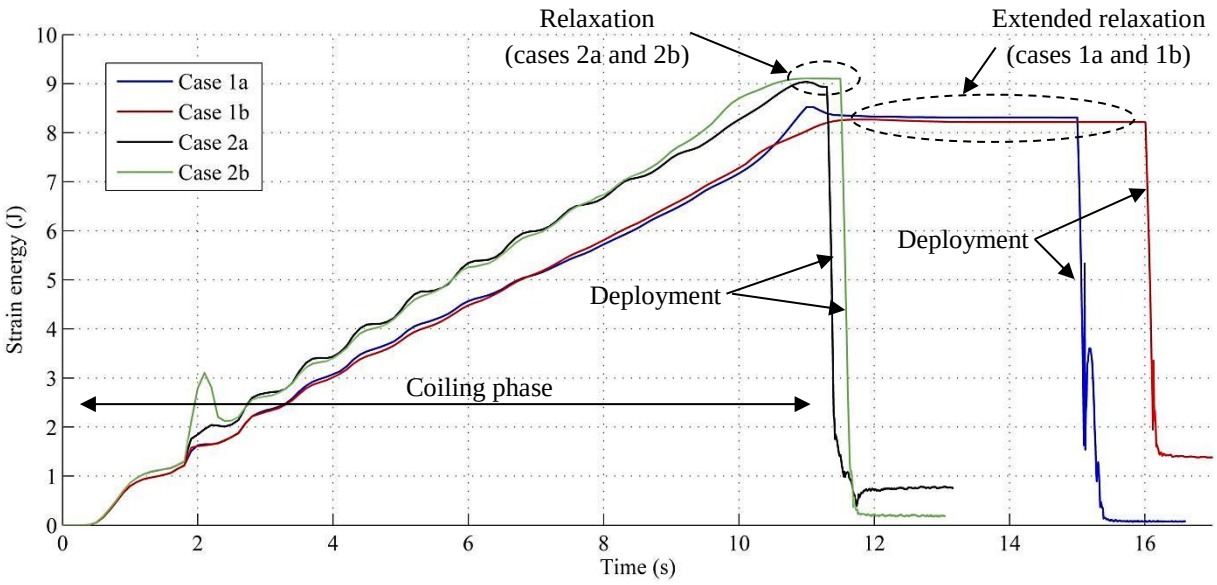

Figure 14. Strain energy for the four cases studied (whole simulation).

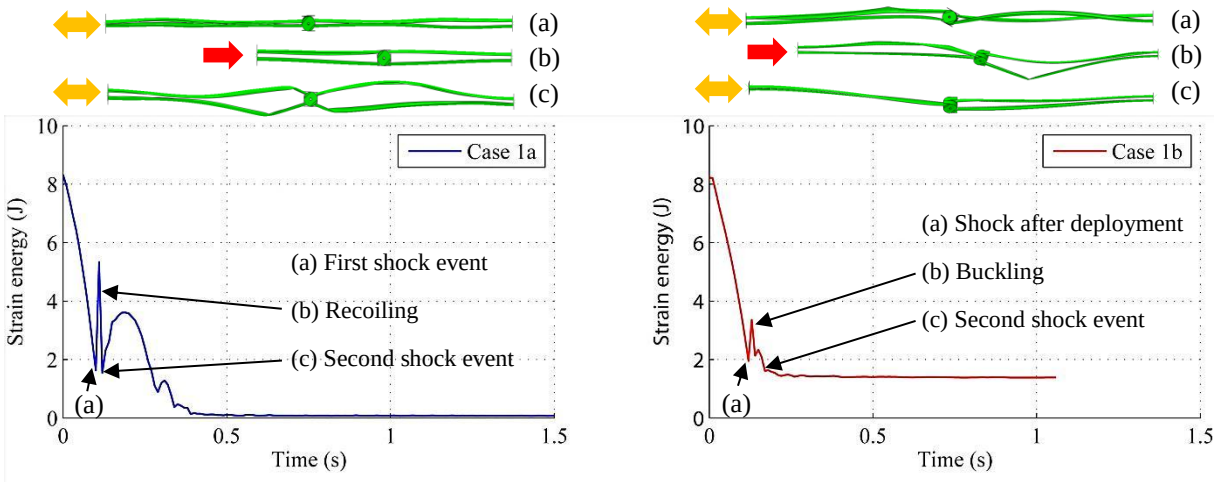

Figure 15. Strain energy plots of cases 1a and 1b (deployment phase only).

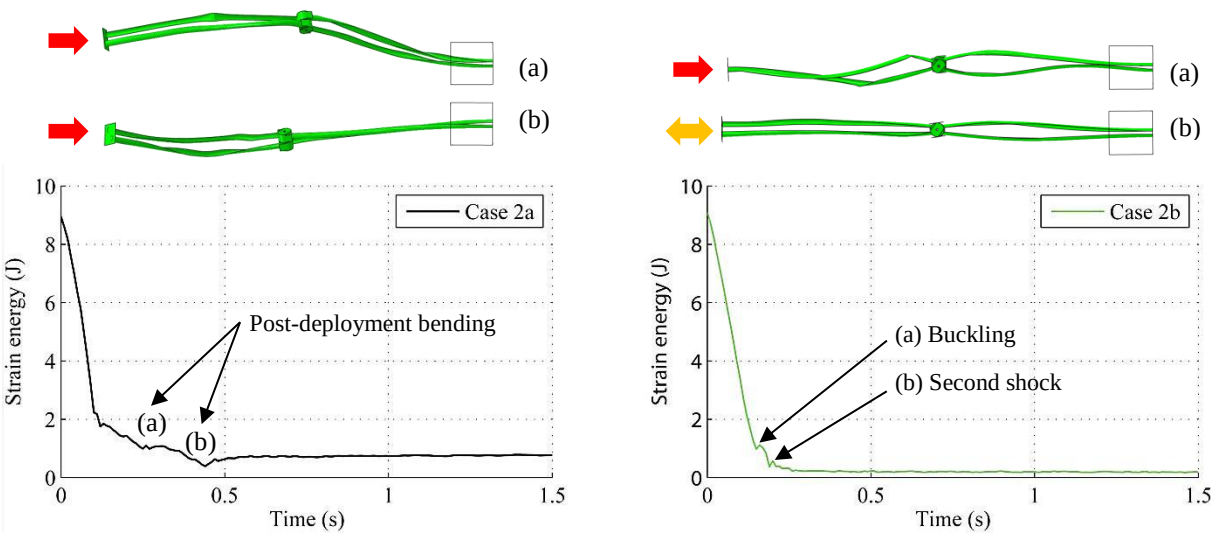

Figure 16. Strain energy plots of cases 2a and 2b (deployment phase only).

K. Deployment time

The deployment time for the boom can be estimated by a simplified mechanical model, Fig. 17. As the back plate, container, and tip plate are rigidly connected by the tape springs, the speed of the tip plate is twice the speed of the container. At time t, the total kinetic energy for the system in Fig. 17 is

$$T = \frac{1}{2}\left[\left(\frac{m_{\text{container}}}{2} + m_{\text{spool}}\right)(R_c\dot{\theta})^2 + \frac{m_{\text{tip}}}{2}(2R_c\dot{\theta})^2 + \left(I_{\text{spool}} + 2I_{\text{tape}}\right)\dot{\theta}^2 + \left(R_{cf} + R_c\theta\right)\chi_{\text{tape}}(2R_c\dot{\theta})^2\right] \tag{2}$$

where θ is the uncoiling angle. The coiling radius R_c varies with the coiling angle $\phi = \phi_{cf} - \theta$, Eq. (3), so for a full coiled tape spring of length L_{tape}, the final coiling angle is found with Eq. (4).

$$R_c = R_{c0} + h_{\text{tape}}/2 + 2h_{\text{tape}}\phi/2\pi \tag{3}$$

$$\phi_{cf} = \frac{\pi}{h_{\text{tape}}}\left[-\left(R_{c0} + \frac{h}{2}\right) + \sqrt{\left(R_{c0} + \frac{h}{2}\right)^2 + \frac{2L_{\text{tape}}h_{\text{tape}}}{\pi}}\right] \tag{4}$$

The inertia of one coiled tape spring, I_{tape}, is thus

$$I_{\text{tape}} = \int_0^{\phi} \chi_{tape} R_c^3 \, \mathrm{d}\phi \tag{5}$$

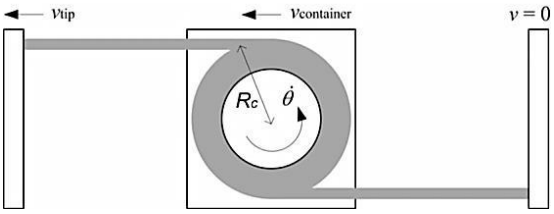

Figure 17: Mechanical model for estimating the deployment time.

To simplify the total kinetic energy, Eq. (2), the magnitude of each term is analyzed with the following data: $m_{\text{container}}$ = 0.0355 kg, m_{spool} = 0.0077 kg, m_{tip} = 0.048 kg, I_{spool} = $8.6\cdot10^{-7}$ kgm^2, R_{c0} = 10 mm, h_{tape} = 0.24 mm, χ_{tape} = 0.004 kg/m (0.2 kg/m^2), L_{tape} = 450 mm, R_{cf} = 13.1 mm. Hence, we have the following inertia terms as percent of total inertia: $(m_{\text{container}}/2+m_{\text{spool}})R_{cf}^2$ = 18.6%, $2m_{\text{tip}}R_{cf}^2$ = 70.2%, I_{spool} = 3.7%, $2I_{\text{tape},cf}$ = 2.1% and

$4(R_{cf}+L_{\text{tape}})\chi_{\text{tape}}\ R_{cf}^{\ 2}$ = 5.4%. Thus, the inertia of the spool and the tape spring are neglected. The total kinetic energy simplifies to

$$T = \frac{1}{2}\left[\left(\frac{m_{\text{container}}}{2} + m_{\text{spool}}\right) + 2m_{\text{tip}}\right]R_c^2\dot{\theta}^2 \tag{6}$$

The strain energy U stored in a tape spring is released in the transition zone and the release rate per length is dependent on the coiling radius, Eq. (3). To avoid the uncoiling angle dependency in the strain energy, it is assume that the strain energy release rate is constant throughout deployment, i.e. $Q(\theta) = Q$. Hence, the release rates for $R_c = R_{c0}$ and $R_c = R_{cf}$ are used in the analysis to get the bounds for the deployment time. The Lagrange equation for the system is written

$$-\frac{\mathrm{d}}{\mathrm{d}t}\left(\frac{\partial T}{\partial \dot{\theta}}\right) + \left(\frac{\partial T}{\partial \theta}\right) + 2Q = 0 \tag{7}$$

as we have two tape springs in the simple model in Fig. 17. Inserting the simplified kinetic energy yields

$$-\left(\frac{m_{\text{container}}}{2} + m_{\text{spool}} + 2m_{\text{tip}}\right)R_{ci}^2\ddot{\theta} + 2Q = 0 \tag{8}$$

which has the solution

$$\theta(t) = \frac{2Q}{\left(m_{\text{container}}/2 + m_{\text{spool}} + 2m_{\text{tip}}\right)R_c^2}\frac{t^2}{2} \tag{9}$$

so for a fully coiled system, the deployment time is

$$t_d = \sqrt{\frac{R_c^2\phi_{cf}}{Q}\left(\frac{m_{\text{container}}}{2} + m_{\text{spool}} + 2m_{\text{tip}}\right)} \tag{10}$$

For a given value of the total strain energy U, the strain energy release per unit length is $U/4L_{\text{tape}}$. The upper and lower bounds for the strain energy release per unit angle are thus $Q_{\max} = UR_{cf}/4L_{\text{tape}}$ and $Q_{\min} = UR_{c0}/4L_{\text{tape}}$. For a total strain energy of U = 9.1 J (Table 3), we have $Q_{\max}$ = 9.1·0.0131/(4·0.450) = 0.066 J and $Q_{\min}$ = 9.1·0.010/(4·0.450) = 0.051 J. Inserting these values in Eq. (10) gives a deployment time between 0.10 and 0.11 s which also agrees well with the simulated deployment times: 0.11-0.15 s, Table 3.

L. CubeSat longitudinal displacement during deployment

Another useful analytical estimation is to calculate the CubeSat displacement during the deployment phase. Conservation of momentum says that the global center of mass (CoM) must not change in a closed system thus one can estimate how much the satellite will translate during deployment in an on-orbit scenario and Abaqus free-free simulations. The generalized expression for finding the CoM position of a system of particles in a 1D problem is shown in Eq. (11). If we take as origin the CoM location of the whole system in our case, Fig. 18, $x_{\text{CoM}} = 0$ in Eq. (11) and d_x is easily found, Eq. (12).

$$x_{\text{CoM}}\sum_{i=1}^{N} m_i = \sum_{i=1}^{N} m_i x_i \tag{11}$$

$$m_{\text{tip}}\left(d_x - L\right) + m_{\text{pair1}}\left(d_x - \frac{3}{4}L\right) + \left(m_{\text{container}} + m_{\text{spools}}\right)\left(d_x - \frac{1}{2}L\right) + m_{\text{pair2}}\left(d_x - \frac{1}{4}L\right) + m_{\text{CubeSat}}d_x = 0 \tag{12}$$

Given the masses from Table 2, we find that the expected longitudinal displacement of the boom with respect to the CoM of the system is d_x = 25.4 mm. This value agrees well with the CubeSat displacement values found in the simulations, Table 3, indicating that the explicit dynamics simulations fulfils the mechanical laws reasonably well.

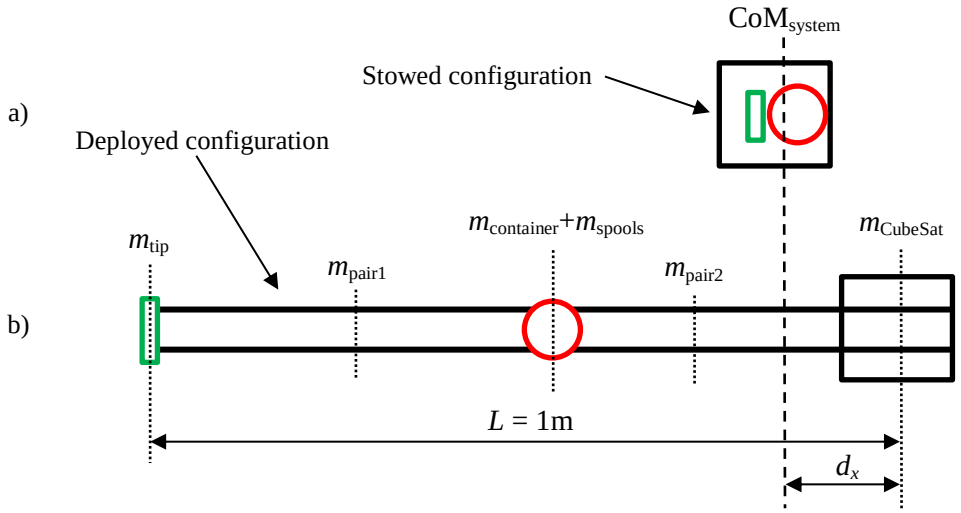

Figure 18. Boom and CubeSat prior deployment, a), and after deployment, b). *Scheme not to scale.*

M. Free tip and container displacements during deployment

The Abaqus simulations showed the fact that the boom tip and container displacements are much greater in the vertical direction than transversely, except in the frictionless standalone boom case (1a), Fig. 19. It is important to mention that the vertical displacements in cases 2a and 2b include the CubeSat rigid body displacements as it is free to move but the overall CubeSat translations during deployment are very small (less than 0.5 mm in both cases). In Figs. 19 and 20 it is also shown that the tip and container in case 1a deploys almost completely straight, that seems to avoid the tape springs buckling but recoiling after the first deployment shock.

The free tip and container are the two masses that are most affected by a GOLS and they need to be properly off-loaded to observe realistic boom dynamics. The weakest bending direction of the boom is known to be in the vertical plane YZ which agrees with the observations from Figs. 19 and 20. It is clear that the vertical displacements are significantly larger than the transversal ones in most cases, especially in the boom tip, and need to be taken into account in future GOLS designs.

N. Kinetic energy

The Abaqus simulations also showed interesting features in the kinetic energy plots. First, the expected decrease in kinetic energy levels at the shock in the cases with friction, Fig. 21. More in detail, Fig. 22, the kinetic energy plots of cases 1a and 1b also show the recoiling phase (1a) and buckling (1b) after the first shock event. Note that the boom recoils almost half of its length. This is believed to be a consequence of a completely straight deployment: the direction of the tip and container reaction forces caused by the shock event is aligned with the tape springs which, instead of buckling them, generate a coiling moment in the spools thus recoiling**.** Both cases show a second shock of lower magnitude.

In the models with the CubeSat the kinetic energy plot of case 2a, Fig. 22, still shows a violent shock, which causes the bending of the boom and the spring back of the tip against the CubeSat (detailed snapshots of this scenario are shown in a posterior section). Case 2b shows the lowest and smoothest kinetic energy peak of all four simulations.

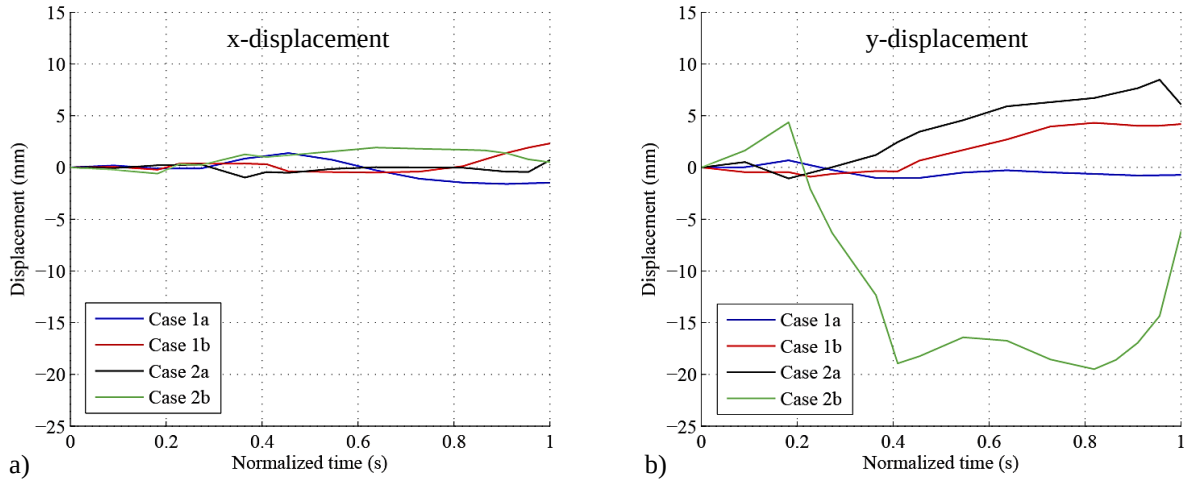

Figure 19. Transversal (x) and vertical (y) boom tip displacements during deployment. *All simulated cases are plotted with the original displacements normalized to a 1 s deployment.*

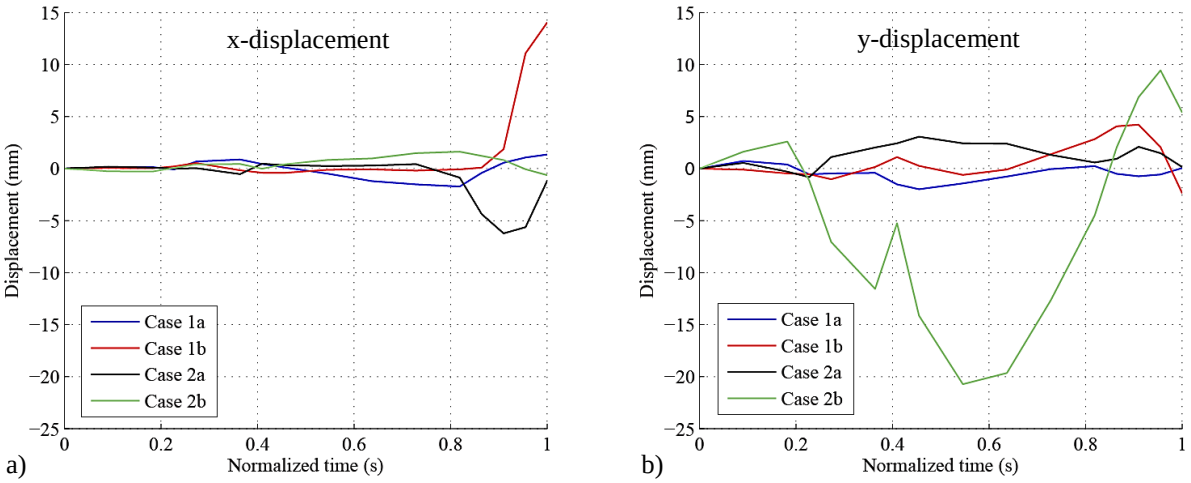

Figure 20. Transversal (x) and vertical (y) container displacements during deployment. *All simulated cases are plotted with the original displacements normalized to a 1 s deployment.*

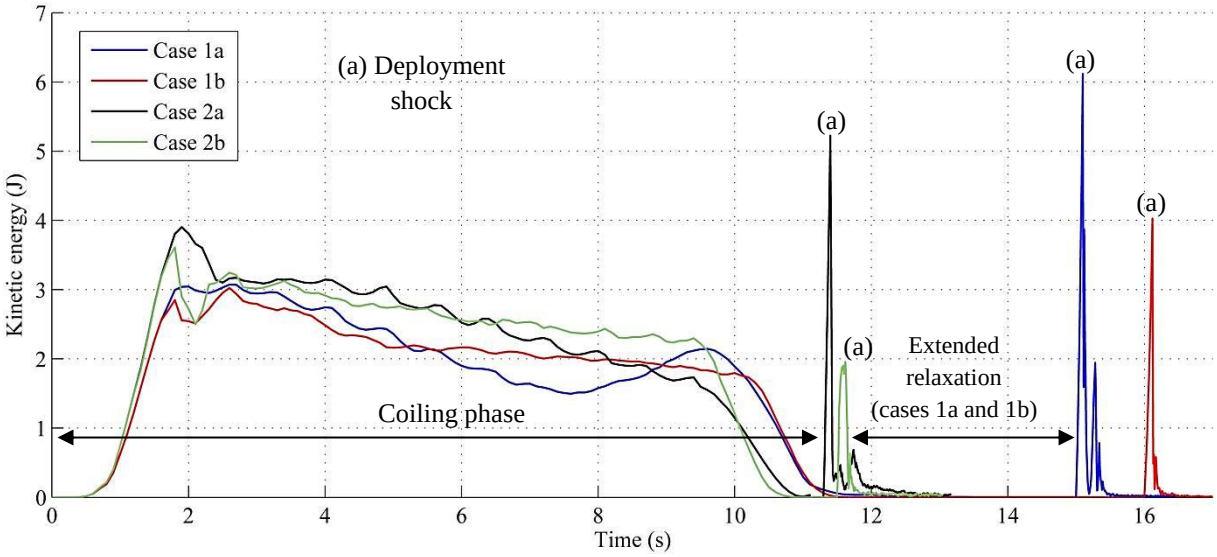

Figure 21. Kinetic energy for all four cases studied (whole simulation).

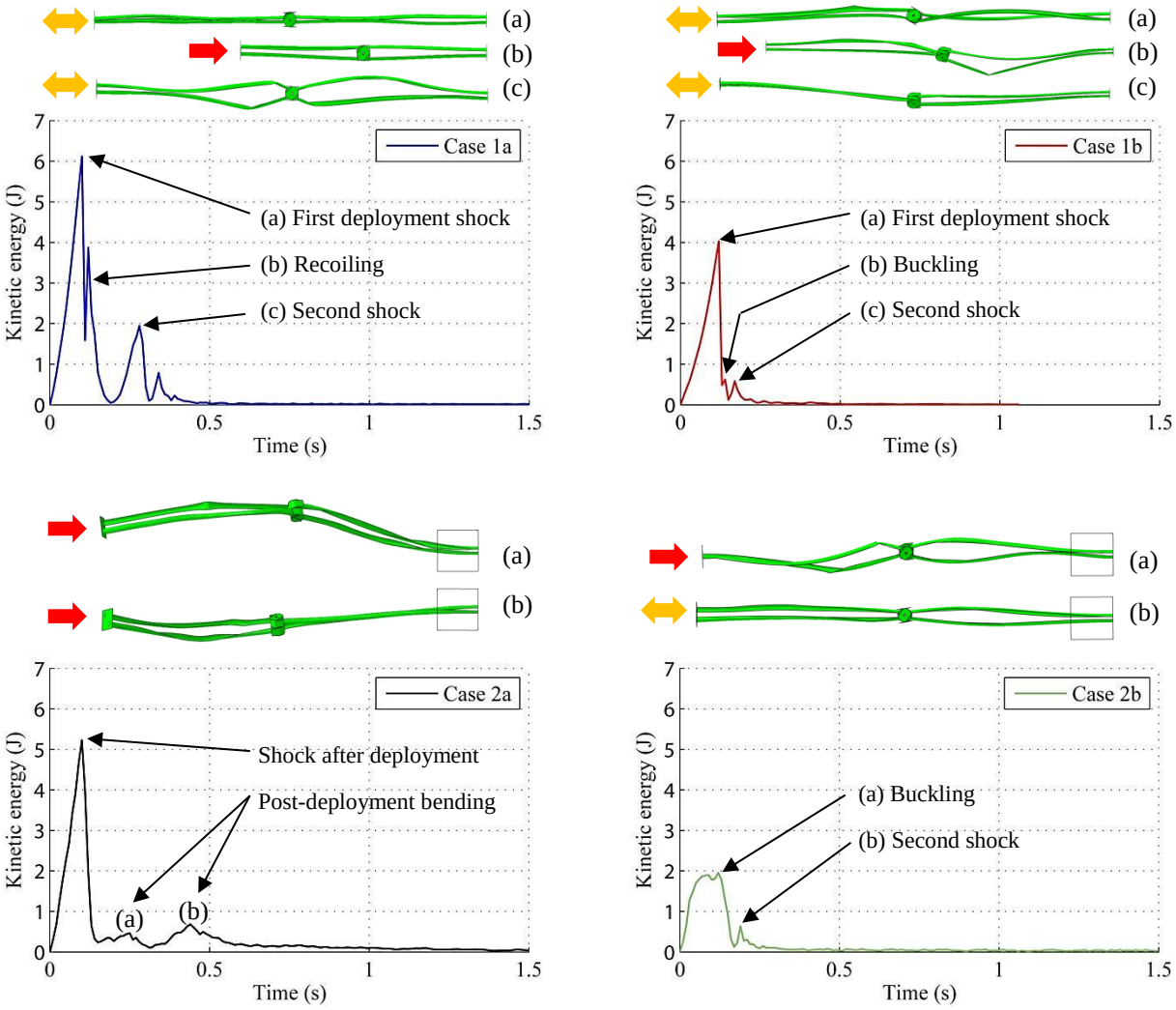

Figure 22. Kinetic energy for the four cases studied (deployment phase only).

O. Deployment and post-deployment dynamics

In this section detailed sequences of the deployment and post-deployment phases for the simulated cases are compared. Figure 23 depicts the stowed configuration prior deployment. The black triangular mark shows the same reference point location and is used throughout the sequences to show how the CubeSat translates in the YZ plane (cases 2a and 2b). In the same Fig. 23 the legend used in the sequences is included to quickly identify the relevant events. Between t = 0 s, deployment start, and t = 0.30 s, Figs. 23–29, only relevant snapshots are shown. After t = 0.30 s the sequence interval is 0.25 s until a total time of 1.25 s, Figs. 30–33.

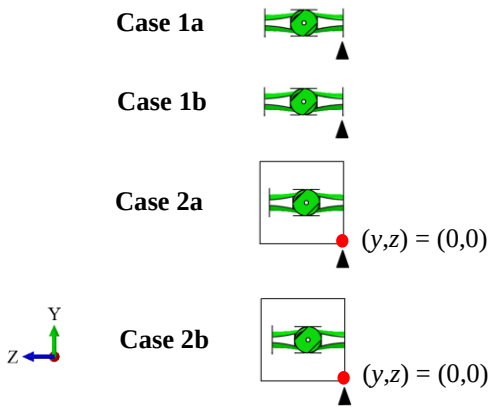

Figure 23 . The four cases stowed prior deployment (t = 0 s). *The initial longitudinal position of the boom attachment plate is marked to highlight the CubeSat displacements.*

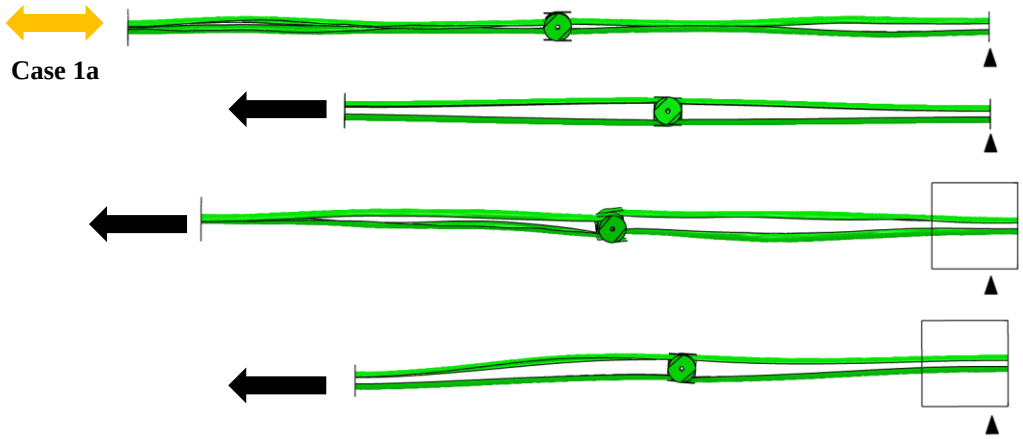

Figure 24. End deployment and shock event of case 1a (t = 0.11 s). *The rest of models keep uncoiling. Note the already clear CubeSat displacements in cases 2a and 2b.*

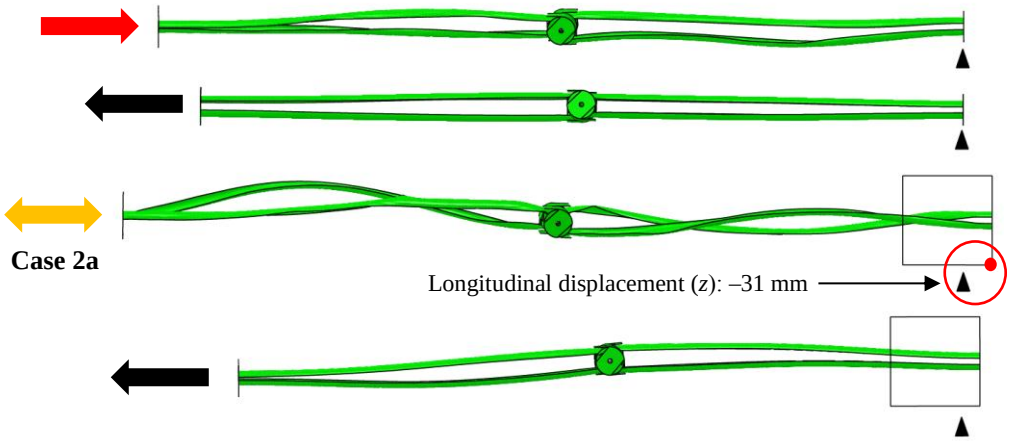

Figure 25. End deployment and shock event of case 2a (t = 0.12 s). *Case 1a recoils after the deployment shock event.*

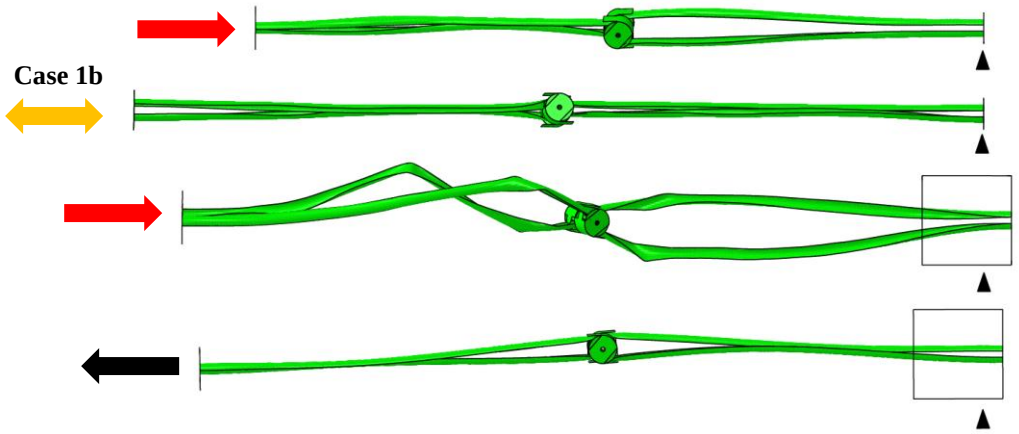

Figure 26. End deployment and shock event of case 1b (t = 0.13 s). *Case 1a keeps recoiling.*

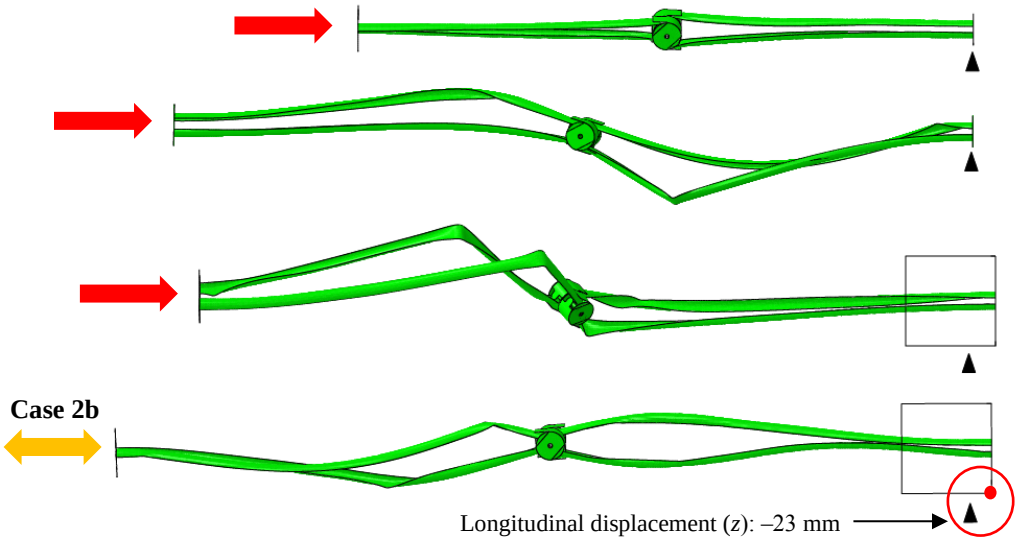

Figure 27. End deployment and shock event of case 2b (*t* = 0.15 s). *Case 1a recoils until half of the total boom length.*

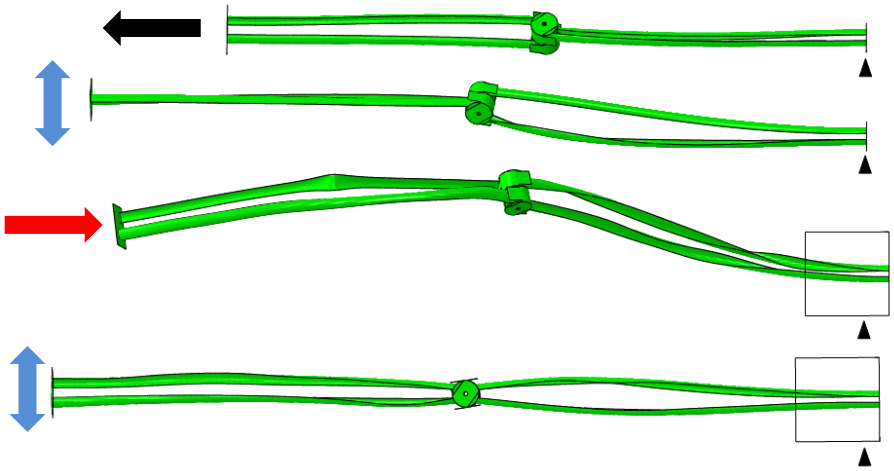

Figure 28. Deployment of case 1a after recoiling (*t* = 0.25 s). *Case 2a remains highly bent while 1b and 2b reach the damped post-deployment phase.*

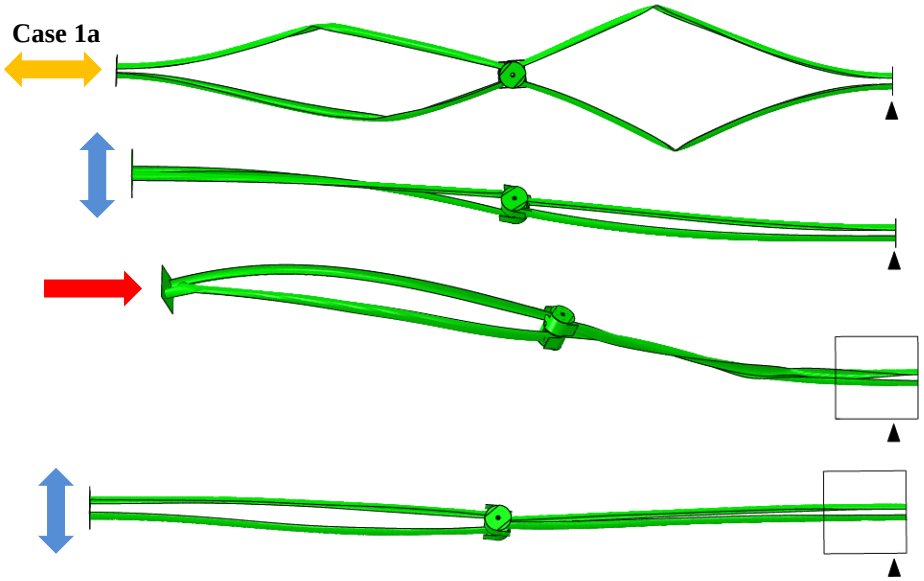

Figure 29. End of second deployment case 1a (*t* = 0.30 s).

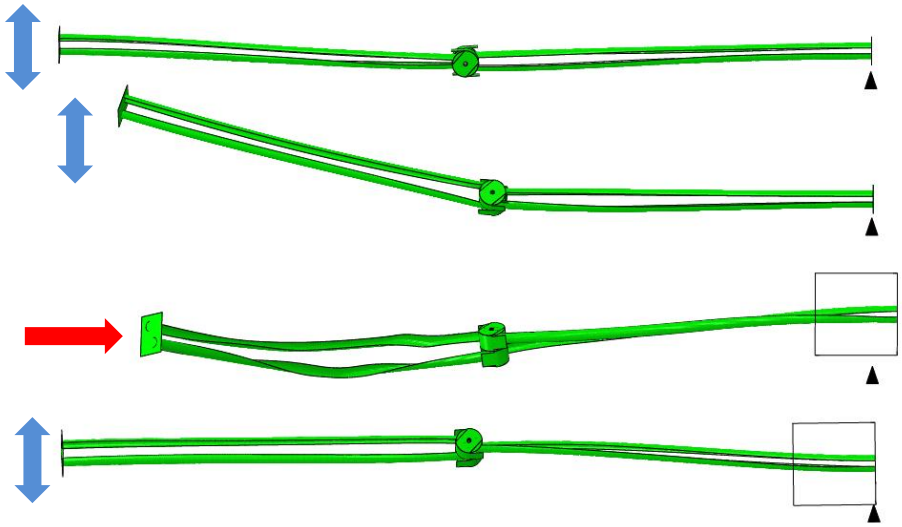

Figure 30. Case 2a continues bending towards the CubeSat (*t* = 0.50 s). *The rest of cases remain in the damped phase.*

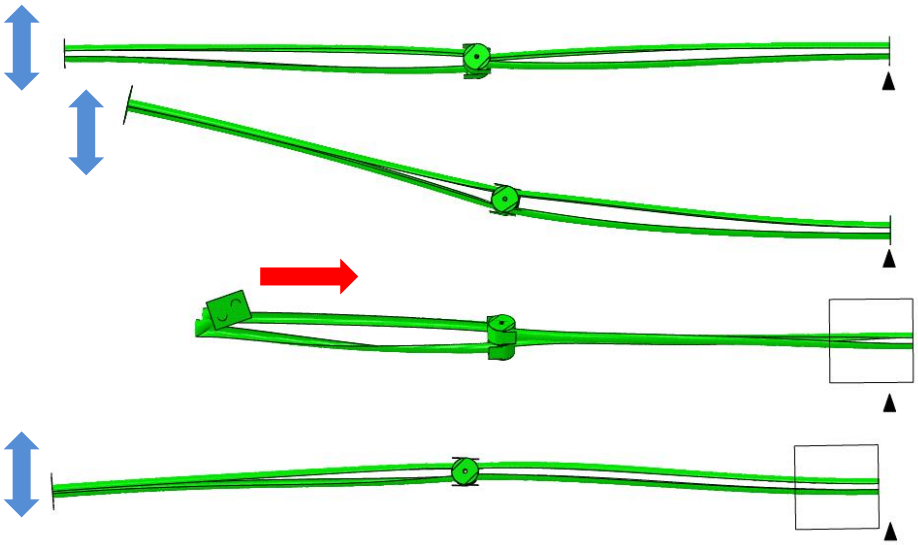

Figure 31. Case 2a continues bending towards the CubeSat (*t* = 0.75 s).

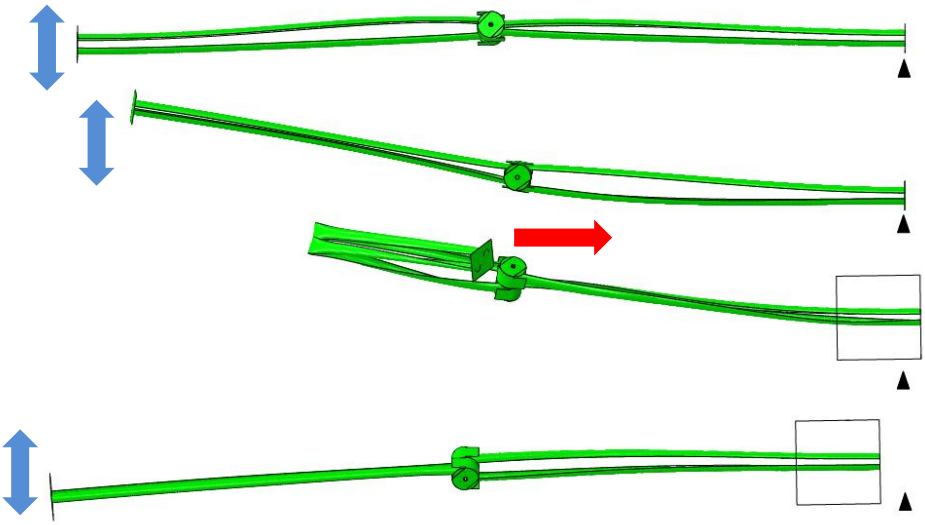

Figure 32. Case 2a continues bending towards the CubeSat (*t* = 1 s).

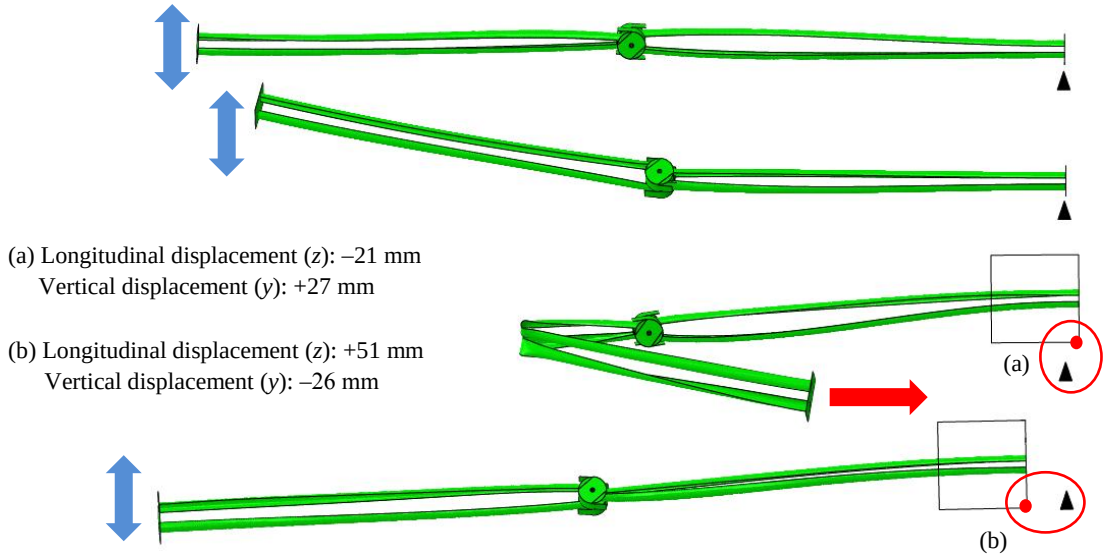

Figure 33. Case 2a continues bending towards the CubeSat (*t* = 1.25 s).

VI. Discussion

P. Analytical models.

The analytical model used to estimate the total strain energy stored after coiling gives a significantly higher value than in the simulations: an over-estimation of around 40 % in the standalone boom and around 30 % for the models with CubeSat. The analytical models verified that the Abaqus models capture well the process of stowing the tape springs, e.g. realistic strain energy levels in the stowed configuration. The models to find estimators for the deployment time and CubeSat longitudinal displacement during deployment agree well with the Abaqus results. In all cases the models show that the simulations are consistent with the considered mechanical laws.

None of the analytical models include friction, which is a factor that plays an important role in the boom dynamics and deployment time but the latter still agrees well with the simulations, especially the two frictionless scenarios (cases 1a and 2a).

The material properties D_{12}, D_{13}, and D_{23} used in the analytical models have also a significant impact on the results and possibly are one of the main reasons of the over-estimation of the stored strain energy. Nevertheless, the current model can be used to show how sensitive the estimated deployment time is to changes in, for example, the material properties D_{12}, D_{13}, and D_{23}. Improvements in the material model used in Abaqus will, most likely, improve the actual results obtained with the strain energy analytical model

Q. Abaqus models

The current FEA model has shown the ability to properly simulate the complex coiling and deployment phases. The analytical model to estimate the stored strain energy and deployment time in the boom agrees reasonably well with the Abaqus simulations. It does not, however, agrees with the deployment time seen during experimental tests, mainly due to not having a detailed material and friction models. The boundary conditions are important for the shock phase and post-deployment behavior.

Note that cases 1a and 2b, Fig. 14, conserve total steady strain energy values of 0.07 and 0.17 J, respectively, in the tape springs. Case 2a did not really reached a steady state phase since the free tip sprang back after the shock event and continued bending the boom until it crashed into the CubeSat model. Case 1b, however, did reach a steady state phase but conserving 1.38 J of strain energy. The reason of why the boom in case 1b remained slightly bent, Figs. 30–33, is unclear. In Fig. 33 it is clearly seen that case 2b displaces towards the deployment direction (Z+) and downwards (Y–). By conservation of momentum these displacements should not be as significant as they are and this effect has not been further analyzed.

The material model needs to be further adjusted in order to mimic the real boom mechanical properties, especially relevant are the out-of-plane properties and Poisson's ratio since they determine the bi-stable characteristics of the laminate. The current model used matches relatively well the out-of-plane properties but not the in-plane ones. [20]

Models with and without friction were run. In all cases the deployment time increases when friction was added to the model, as expected. The finite element models with friction have a friction coefficient of 0.2 between tape springs themselves and the container part.

There are several friction formulations available, e.g. penalty and static-kinetic exponential decay, which should be carefully investigated in the future. The pairs of surfaces where non-zero friction is implemented are also another important aspect to consider and not trivial.

Figure 2[1] shows that when the boom was fixed in one end, the first shock event was much more violent, as expected. The less strain energy stored in those models compared with the ones with CubeSat, Fig. 14, approximately 7 % less in the frictionless case and around 10 % less in the case with friction, seemed not to have as much effect in the shock kinetic energy levels as the boundary conditions. The reason is that in the free-free deployments with CubeSat, the model can dissipate the shock kinetic energy by either buckling the tape springs or transferring momentum to the CubeSat. In the standalone boom models all the dissipation has to be taken by the tape springs. An interesting case is when the reaction forces of the tip at the shock are aligned with the main boom axis, case 1a in Figs. 25–27: instead of buckling the tape springs we observed that this balanced forces scenario provoked a moment large enough in the spools so that they allowed the boom to recoil.

R. Experimental tests

The used GOLS has several limitations. First, the springs are activated when the boom rotates in the horizontal plane. This aspect is in the process of being mitigated using a two levels Marionette system. [21] Abaqus models have already been run to assess the Marionette system's applicability and it is planned to implement this solution in the near future. [14]

The data we have collected is mainly based on post-processing of videos up to 60 fps. Although great care has been taken when analyzing the video frames, improvements on the data acquisition part are expected to happen also in the future.

VII. Conclusion

We currently cannot obtain complete detailed quantitative comparisons between our simulations and the experimental tests, mainly because:

1) The material model needs to be improved and verified.
2) Frictional aspects must be addressed in detail and reformulated in the Abaqus models.
3) No Gravity Off-Loading System was included in any of the Abaqus models.
4) Some DOFs are not completely free in the used GOLS.
5) Experimental data quality: a better set-up needs to be implemented, i.e. using of sensors or a motion capture system.

We can, however, confirm that the FEA models are capturing properly the main mechanical and physical features of such complex deployable system.

The next steps from the modeling point of view are to include a better friction formulation and improve the material model. These two aspects should provide valuable insight on material modeling of thin woven composites for FEA use and frictional aspects in modeling complex deployable structures. Without a significant change in the stored strain energy the improved models should show a dramatic increase in the deployment time: experimental tests showed a deployment time of 1.03 s and the FE models 0.11–0.15 s. Friction is, however, very hard to analyze and verify.

Other modeling aspects that might be of great importance are the use of damping and creep. Abaqus has readily available the implementation of material damping but it was not investigated. Material creep had an enormous impact on the bi-stability characteristics of our CFRP tape springs: after few hours coiled the tape springs became neutrally stable due to matrix creep, e.g. they have the same strain energy in both coiled and straight configurations, and they do not show any preferred deployment direction. This effect did not prevent us from experimentally test the boom deployment but it is a problem that certainly needs to be addressed for any system implementation.

An improved GOLS has already been modeled but not included in the boom models. When both models are merged, the new complete model will permit a better comparison between FEA and experiments, especially from the dynamics point of view. It will also give us the opportunity to assess the capability of the gravity-off-loading strategy and to assess further improvements in the FEA environment, saving time, human resources, and costs.

Acknowledgments

We thank Drs. Hien Bich Vo (IAUPR), Gloria Wiens (UF), and Nickolay Ivchenko (KTH) for inviting us to the SWIM CubeSat project. Special thanks go to Dr. Thomas W. Murphey (AFRL) for the interesting discussions and guidance on deployable structures, tape springs, testing, and simulations and for the kind invitation to assist him during the deployment tests of the real SIMPLE boom at AFRL in autumn 2012.

We also thank M.S. Adam Biskner and M.S. Greg Sanford at LoadPath for making the trip at AFRL possible and acknowledge the important simulation and testing contributions from KTH's master students M.S. Yoann Prigent, M.S. Valeriy Shepenkov, and Mr. Julien Servais.

References

[1] "6U CubeSat Low Cost Space Missions", Workshop presentation, Australian Center for Space Engineering Research, AITC, Mt. Stromlo Observatory, Canberra, Australia, URL: www.acser.unsw.edu.au/events/cubesat.html, 17–18 July 2012.

[2] Klofas, B., "CubeSat Communications Survey Update", Workshop presentation, Summer Developer's at Utah State University, 2011.

[3] Ivchenko, N., Small Explorer for Advanced Missions (SEAM), Research proposal to European Commission FP7 Work Programme SPA.2013.3.1-01: SME space technology research and technology transfer, November 21, 2012 (unpublished).

[4] Tibert, G. "Deployable Tensegrity Structures for Space Applications," Ph.D. Dissertation, Mechanics Dept., Royal Institute of Technology (KTH), Stockholm, 2002.

[5] Mangenot, C., Santiago-Prowald, J., Kees van't kloster, Fonseca, N., Scolamiero, L., and Coromina, F., "Large Reflector Antenna Working Group – Final Report," European Space Agency (ESA), Document reference TEC-EEA/2010.595/CM, September 8, 2010.

[6] Thomas, G. M., "Prototype Development and Dynamic Characterization of Deployable CubeSat booms," M.S. Thesis Aeronautics and Astronautics Dept., Air Force Institute of Technology (AFIT), Wright-Patterson Air Force Base, OH, 2012.

[7] Swenson, P. H., Thomas, G. M., Cobb, R. G., Black, J. T., and Swenson, E. D., "Development and Design of an AFIT CubeSat Demonstrating Deployable Technology," *51st AIAA/ASME/ASCE/AHS/ASC Structures, Structural Dynamics, and Materials Conference*, 12–15 April 2010, Orlando, FL, AIAA-2010-2906.

[8] Sickinger, C., Herbeck, L., and Breitbach, E., "Structural Engineering on Deployable CFRP Booms for a Solar Propelled Sailcraft", *Acta Astronautica*, Vol. 58, No. 4, 2006.

[9] Keller, P. N., Lake, M. S., Francis, W., Harvey, J., Winter, J., et al., "Development of a Deployable Boom for Microsatellites Using Elastic Memory Composite Material," *45th AIAA/ASME/ASCE/AHS/ASC Structures, Structural Dynamics, and Materials Conference*, 19–22 April 2004, Palm Springs, CA, AIAA-2004-1603.

[10] Jeon, S. K., and Murphey, T. W., "Design and Analysis of a Meter-Class CubeSat Boom with a Motor-Less Deployment by Bi-Stable Tape Springs," *52nd AIAA/ASME/ASCE/AHS/ASC Structures, Structural Dynamics, and Materials Conference*, Denver, CO, 4–7 April 2011, AIAA-2011-1731.

[11] Vo, H. B., "Space Weather Ion Measurement – SWIM Preliminary Design Review," Presentation in the Preliminary Design Review at IAUPR, 2011 (unpublished).

[12] Iqbal, K. and Pellegrino, S. "Bi-stable composite shells," *41st AIAA/ASME/ASCE/AHS/ASC Structures, Structural Dynamics, and Materials Conference and Exhibit*, 3–6 April 2000, Atlanta, GA, AIAA-2000-1385.

[13] Prigent, Y., Mallol, P., and Tibert, G., "A Classical Lamination Model of Bi-Stable Woven Composite Tape-Springs," *24th Nordic Seminar on Computational Mechanics (NSCM*) edited by J. Freud and R. Kouhia, pp. 51-54, Helsinki, 2011.

[14] Shepenkov, V., "Vibration Modal Analysis of a Deployable Boom Integrated to a CubeSat," M.S. Thesis, Mechanics Dept., Royal Institute of Technology (KTH), 2012.

[15] Murphey, T. W., Jeon, S. K., Biskner, A., and Sanford, G., "Deployable Booms and Antennas Using Bi-stable Tape-springs," *24th Annual AIAA/USU Conference on Small Satellites*, 9–12 August 2010, Logan, UT.

[16] Tibert, G., Mallol, P., Shepenkov, V., and Servais, J., "Deployment Dynamics Tests of Boom," Presentation in the Critical Design Review at AFRL, 2012 (unpublished).

[17] TexGen, geometry modelling of textile structures, Software Package, Ver. 3.5.2, University of Nottingham, 2012.

[18] Stig, F., "3D-Woven Reinforcement in Composites," Ph.D. Dissertation, Aeronautical and Vehicle Engineering Dept., Royal Institute of Technology (KTH), Stockholm, 2012.

[19] Kueh, A.B.H., and Pellegrino, S., "ABD Matrix of Single-Ply Triaxial Weave Fabric Composites," *48th AIAA/ ASME/ASCE/AHS/ASC Structures, Structural Dynamics, and Materials Conference*, 23–26 April 2007, Honolulu, Hawaii, AIAA-2007-2161.

[20] Prigent, Y., "Finite Element Model of Bi-Stable Woven Composite Tape-Springs," M.S. Thesis, Mechanics Dept., Royal Institute of Technology (KTH), Stockholm, 2011.

[21] Greschik, G., and Belvin, W. K., "High-Fidelity Offloading System for Free-Free Vibration Testing," *Journal of Spacecraft and Rockets* Vol.44, No. 1, January–February 2007.